Thin-Walled Structures 143 (2019) 106224

Contents lists available at ScienceDirect

Thin-Walled Structures

journal homepage: www.elsevier.com/locate/tws

Full length article

An isogeometric formulation for stability analysis of laminated plates and shallow shells

Jamires Sousa Cordeiro Praciano[a], Pedro Sanderson Bastos Barros[a], Elias Saraiva Barroso[a,b], Evandro Parente Junior[a,*], Áurea Silva de Holanda[c], João Batista M. Sousa Junior[a]

[a] Laboratório de Mecânica Computacional e Visualização, Departamento de Engenharia Estrutural e Construcão Civil, Universidade Federal do Ceará, Fortaleza, CE, Brazil
[b] Computer Graphics, Virtual Reality and Animation Group (CRAb), Departamento de Computação, Universidade Federal do Ceará, Fortaleza, CE, Brazil
[c] Departamento de Integração Acadêmica e Tecnológica, Universidade Federal do Ceará, Fortaleza, CE, Brazil

ARTICLE INFO

Keywords:
Isogeometric analysis
NURBS
Composite materials
Laminated structures
Post-buckling behavior

ABSTRACT

Laminated composite plates and shells have been widely used in aeronautical, mechanical, and naval structures. Stability is a major concern in the design of these structures due to their high slenderness. Therefore, it is necessary to properly analyze their post-critical behavior, assessing their sensitivity to initial imperfections and load-carrying capacity. This paper presents a methodology based on the Isogeometric Analysis to study the stability of laminated plates and shallow shells. In this formulation, the geometry and displacement field are described using NURBS basis functions. Appropriate integration schemes are used to avoid the locking problem for thin-walled plates and shells. The proposed formulation was applied in the stability analysis of various examples and excellent results were obtained. The influence of the composite layup and geometric imperfections on the buckling load and post-critical behavior is studied. New bifurcation solutions to a well-known laminated shell buckling benchmark problem are presented.

1. Introduction

Fiber reinforced composite materials present high mechanical performance and low weight, high corrosion and fatigue resistance, and good structural damping. These characteristics are responsible for the increase of the application of composite materials in engineering. In particular, composite plates and shells have been widely used in manufacturing structural components for aeronautical, mechanical, and naval engineering applications. Due to the practical importance of these structures, the development of analysis methods to composite plates and shells is a very active research field [1–9].

The Isogeometric Analysis (IGA) is a recent numerical method that uses for displacement approximation the same functions used for geometric modeling by CAD programs [10–18]. The discretization of the isogeometric model can be easily carried out using well-known techniques from geometric modeling, as knot insertion and degree elevation [19]. Moreover, it is possible to use a new discretization approach, different from the h and p refinements used in the Finite Element Method (FEM), known as k refinement, which increases not only the basis order but also the continuity between adjacent elements. Thus, there is an ongoing effort to develop isogeometric formulations for analysis of composite plates and shells [17,20–29].

It is worth noting that structural stability is of paramount importance in the design of laminated plates and shells, as they are usually very slender and prone to buckling [30–33]. Thus, this work presents an accurate and efficient isogeometric formulation for geometrically nonlinear analysis of laminated composite shallow shells based on the Reissner-Mindlin plate theory and Marguerre strains.

The use of NURBS functions allows the exact representation of complex geometries throughout the analysis, independent of the discretization level used to approximate the displacement field. This is an important issue in the stability analysis of thin-walled plates and shells since geometric imperfections have a considerable influence over the obtained results. Thus, errors in the representation of the geometry can lead to incorrect equilibrium paths for imperfection sensitive structures.

The proposed approach allows the modeling of laminated plates (perfect and imperfect) and shallow shells with arbitrary layups. Furthermore, this formulation does not require the use of artificial geometric imperfections in order to study the post-buckling behavior. As shown by the numerical examples, it can analyze perfect and

* Corresponding author. Universidade Federal do Ceará, Laboratório de Mecânica Computacional e Visualização, Departamento de Engenharia Estrutural e Construção Civil, 60440-900, Fortaleza, Ceará, Brazil.
E-mail addresses: jamirescordeiro@gmail.com (J.S.C. Praciano), pedrosanderson88@gmail.com (P.S.B. Barros), elias.barroso@gmail.com (E.S. Barroso), evandro@ufc.br (E. Parente), aurea@det.ufc.br (Á.S.d. Holanda), joaobatistasousajr@hotmail.com (J.B.M. Sousa).

https://doi.org/10.1016/j.tws.2019.106224
Received 30 May 2018; Received in revised form 18 May 2019; Accepted 29 May 2019
Available online 28 June 2019
0263-8231/

imperfect structures, trace complex equilibrium paths, detect buckling points and obtain the secondary paths after bifurcation. In addition, the numerical response can be easily improved using *h*, *p* and *k* refinements.

It is important to note that isogeometric analysis does not eliminate shear locking for fully integrated Reissner-Mindlin elements [34]. In addition, curved shell elements suffer not only shear locking but also membrane locking [35]. However, reduced integration schemes have been successfully used for NURBS-based isogeometric formulations for small displacement analysis [36,37]. In this work, the accuracy of different numerical integrations schemes will be assessed for the stability and nonlinear analysis of plates and shallow shells. The numerical examples show that the use of high regularity basis functions obtained by *k*-refinement and an appropriate reduced integration scheme not only avoids locking but also reduces the computational cost, resulting in a very accurate and efficient approach for nonlinear analysis of laminated plates and shallow shells.

The proposed formulation will be applied in the stability analysis of various examples including the evaluation of the buckling load and post-critical behavior. The influence of the composite layup and geometric imperfections on the buckling load and post-critical behavior will be studied and discussed. New bifurcation solutions to a well-known laminated shell buckling benchmark problem [38] will be presented.

This paper is organized as follows. Section 2 discusses the laminated modeling, including kinematics and sectional forces. Section 3 presents the proposed isogeometric formulation for nonlinear analysis of plates and shallow shells. Section 4 presents the numerical examples and Section 5 presents the main conclusions.

2. Laminated shallow shells

The kinematic formulation for shallow shells adopted here is based on Reissner-Mindlin theory for bending and transverse shear strains and on Marguerre theory for nonlinear membrane strains, including the effect of initial curvatures and moderate rotations. This formulation allows the nonlinear analysis of perfect and imperfect plates and shallow shells in a simpler and more efficient manner than the use of general shell elements [12,16,18]. It is worth noting that the computational efficiency is very important to the optimization of composite structures using bio-inspired algorithms [30–33] since these methods require a large number of structural analyses in order to find the optimum design.

The basic hypothesis of Reissner-Mindlin theory, also known as first-order shear deformation theory (FSDT) [39], is that a straight line, normal to the middle plane of the plate, remains straight but not necessarily normal after deformation, as shown in Fig. 1. Thus, displacement of the plate at any point is given by:

$$\begin{aligned} u_x(x,y,z) &= u(x,y) + z\,\theta_y \\ u_y(x,y,z) &= v(x,y) - z\,\theta_x \\ u_z(x,y,z) &= w(x,y) \end{aligned} \tag{1}$$

where u, v and w are the midplane displacements in the x, y and z directions; θ_x and θ_y are the rotations about x and y axes, respectively. The transverse shear strains are given by:

$$\boldsymbol{\gamma} = \begin{Bmatrix} \gamma_{xz} \\ \gamma_{yz} \end{Bmatrix} = \begin{Bmatrix} w_{,x} + \theta_y \\ w_{,y} - \theta_x \end{Bmatrix} \tag{2}$$

When displacements are moderately large, there is an interaction between membrane and bending effects due to transverse displacements. Using Marguerre theory [40], the in-plane strains are given by:

$$\boldsymbol{\varepsilon} = \begin{Bmatrix} \varepsilon_x \\ \varepsilon_y \\ \gamma_{xy} \end{Bmatrix} = \boldsymbol{\varepsilon}^m + z\,\boldsymbol{\kappa} \tag{3}$$

Where the curvatures are given by

$$\boldsymbol{\kappa} = \begin{Bmatrix} \theta_{y,x} \\ -\theta_{x,y} \\ \theta_{y,y} - \theta_{x,x} \end{Bmatrix} \tag{4}$$

And the membrane strains are

$$\boldsymbol{\varepsilon}^m = \begin{Bmatrix} u_{,x} \\ v_{,y} \\ u_{,y} + v_{,x} \end{Bmatrix} + \begin{Bmatrix} w_{,x}\, z_{0,x} \\ w_{,y}\, z_{0,y} \\ w_{,x}\, z_{0,y} + w_{,y}\, z_{0,x} \end{Bmatrix} + \begin{Bmatrix} \frac{1}{2} w_{,x}^2 \\ \frac{1}{2} w_{,y}^2 \\ w_{,x}\, w_{,y} \end{Bmatrix} \tag{5}$$

where $z_0\,(x, y)$ is the elevation of the shell mid-surface. It is interesting to note that this expression reduces to the von Kármán strains for an initially flat plate ($z_0 = 0$).

The generalized Hooke's Law can be used to obtain the stress-strain relationship in the local system of the ply. For a plane stress condition, the constitutive relation is given by Ref. [39]:

$$\begin{Bmatrix} \sigma_1 \\ \sigma_2 \\ \tau_{12} \end{Bmatrix} = \begin{bmatrix} Q_{11} & Q_{12} & 0 \\ Q_{12} & Q_{22} & 0 \\ 0 & 0 & Q_{66} \end{bmatrix} \begin{Bmatrix} \varepsilon_1 \\ \varepsilon_2 \\ \gamma_{12} \end{Bmatrix} \rightarrow \boldsymbol{\sigma}_1 = \mathbf{Q}_m\, \boldsymbol{\varepsilon}_1 \tag{6}$$

where $\boldsymbol{\sigma}_1$ and $\boldsymbol{\varepsilon}_1$ are the stress and strain vectors at local ply system (Fig. 2) and $\mathbf{Q}_m$ is the elastic constitutive matrix, whose terms are given by:

$$\begin{aligned} Q_{11} &= \frac{E_1}{1-\nu_{12}\,\nu_{21}}; \quad Q_{12} = \frac{\nu_{21}\,E_1}{1-\nu_{12}\,\nu_{21}}; \\ Q_{22} &= \frac{E_2}{1-\nu_{12}\,\nu_{21}}; \quad Q_{66} = G_{12} \end{aligned} \tag{7}$$

In structural analysis, it is necessary to transform the stresses from the ply system to the global one:

$$\boldsymbol{\sigma} = (\mathbf{T}_m^T\, \mathbf{Q}_m\, \mathbf{T}_m)\, \boldsymbol{\varepsilon} = \bar{\mathbf{Q}}_m\, \boldsymbol{\varepsilon} \tag{8}$$

where the transformation matrix ($\mathbf{T}_m$) is given by

$$\mathbf{T}_m = \begin{bmatrix} \cos^2\theta & \sin^2\theta & \sin\theta\cos\theta \\ \sin^2\theta & \cos^2\theta & -\sin\theta\cos\theta \\ -2\sin\theta\cos\theta & 2\sin\theta\cos\theta & \cos^2\theta - \sin^2\theta \end{bmatrix} \tag{9}$$

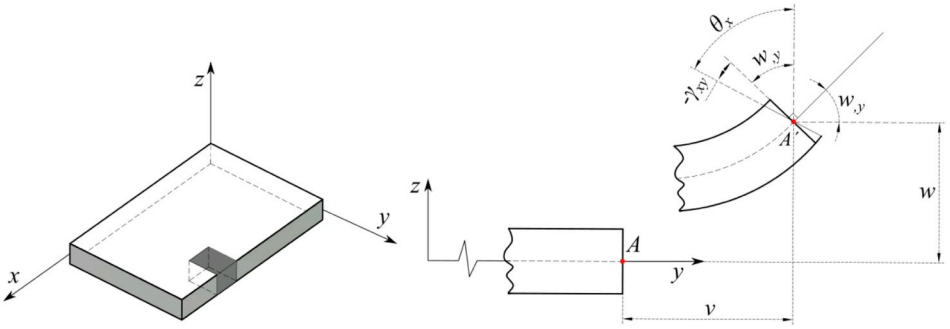

Fig. 1. Initial and deformed geometries.

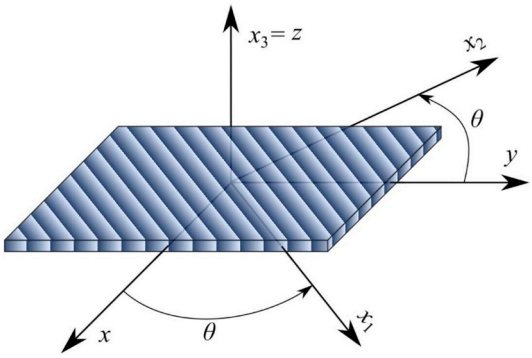

Fig. 2. Local and global coordinate systems for a ply.

The transverse shear stresses in the ply system can be computed from

$$\begin{Bmatrix} \tau_{13} \\ \tau_{23} \end{Bmatrix} = \begin{bmatrix} Q_{44} & 0 \\ 0 & Q_{55} \end{bmatrix} \begin{Bmatrix} \gamma_{13} \\ \gamma_{23} \end{Bmatrix} \rightarrow \tau_1 = \mathbf{Q}_s \, \gamma_1 \tag{10}$$

where $\mathbf{Q}_s$ is the transverse shear constitutive matrix in the local system, whose terms are $Q_{44} = G_{13}$ and $Q_{55} = G_{23}$. These stresses can be transformed to the global system using the expression:

$$\tau = (\mathbf{T}_s^T \, \mathbf{Q}_s \, \mathbf{T}_s) \, \gamma = \bar{\mathbf{Q}}_s \, \gamma \tag{11}$$

where the transformation matrix ($\mathbf{T}_s$) is given by

$$\mathbf{T}_s = \begin{bmatrix} \cos\theta & \sin\theta \\ -\sin\theta & \cos\theta \end{bmatrix} \tag{12}$$

The internal forces and moments are obtained integrating stresses through the laminate thickness:

$$\begin{aligned} \mathbf{N} &= \begin{Bmatrix} N_x \\ N_y \\ N_{xy} \end{Bmatrix} = \int_{-h/2}^{h/2} \begin{Bmatrix} \sigma_x \\ \sigma_y \\ \tau_{xy} \end{Bmatrix} dz \\ \mathbf{M} &= \begin{Bmatrix} M_x \\ M_y \\ M_{xy} \end{Bmatrix} = \int_{-h/2}^{h/2} \begin{Bmatrix} \sigma_x \\ \sigma_y \\ \tau_{xy} \end{Bmatrix} z \, dz \\ \mathbf{V} &= \begin{Bmatrix} V_{xz} \\ V_{yz} \end{Bmatrix} = \int_{-h/2}^{h/2} \begin{Bmatrix} \tau_{xz} \\ \tau_{yz} \end{Bmatrix} dz \end{aligned} \tag{13}$$

Finally, the stress resultants $\hat{\sigma}$ can be written in terms of the generalized strains $\hat{\varepsilon}$ as:

$$\begin{Bmatrix} \mathbf{N} \\ \mathbf{M} \\ \mathbf{V} \end{Bmatrix} = \begin{bmatrix} \mathbf{A} & \mathbf{B} & \mathbf{0} \\ \mathbf{B} & \mathbf{D} & \mathbf{0} \\ \mathbf{0} & \mathbf{0} & \mathbf{G} \end{bmatrix} \begin{Bmatrix} \varepsilon^m \\ \kappa \\ \gamma \end{Bmatrix} \rightarrow \hat{\sigma} = \mathbf{C} \, \hat{\varepsilon} \tag{14}$$

where **A**, **B**, **D** and **G** are the extensional, membrane-bending coupling, bending and shear stiffness matrices, respectively, whose elements are given by:

$$\begin{aligned} A_{ij} &= \sum_{k=1}^{np} \bar{Q}_{ij}^k (z_{k+1} - z_k) \; ; \; B_{ij} = \sum_{k=1}^{np} \frac{\bar{Q}_{ij}^k (z_{k+1}^2 - z_k^2)}{2} \\ D_{ij} &= \sum_{k=1}^{np} \frac{\bar{Q}_{ij}^k (z_{k+1}^3 - z_k^3)}{3} \; ; \; G_{ij} = \sum_{k=1}^{np} k_s \, \bar{Q}_{ij}^k (z_{k+1} - z_k) \end{aligned} \tag{15}$$

where np is and number of plies and k_s is the shear correction factor (taken as 5/6 in this work).

It is worth pointing out that there are three types of membrane-bending coupling in laminated shallow shells: the first due to the effect of the composite layup on **B** matrix, the second due to von Kármán nonlinear strains, and the third due to the initial curvature of the structure. These couplings affect the nonlinear behavior of shallow shells and imperfect plates. An important consequence is that compressed imperfect plates, even with symmetric layups ($\mathbf{B} = 0$), generally do not present bifurcation buckling due to the membrane-bending coupling caused by the initial imperfections.

3. Isogeometric analysis

Isogeometric formulations approximate the displacement field using the same basis functions used by the CAD systems for geometric modeling. This feature not only simplifies the communication between CAD and analysis programs, but also allows the geometry of the structure to be exactly represented, independent of the discretization level adopted in the numerical analysis. This is a major advantage over FEM, where the geometry of the structure is approximated using polynomial basis functions.

3.1. NURBS

Non-Uniform Rational B-Splines (NURBS) are parametric representations widely used in geometric modeling, since they offer a mathematical description capable to represent both analytic and free form surfaces using the same database. Moreover, the use of NURBS allows the exact representation of quadric surfaces, as cylinders, ellipsoids and spheres [19].

A tensor product NURBS surface of degree ($p \times q$) is defined by a linear combination of bivariate rational basis functions (R) and a matrix of control points ($\mathbf{p}$):

$$S(\xi, \eta) = \sum_{i=1}^{m} \sum_{j=1}^{n} R_{ij}(\xi, \eta) \, \mathbf{p}_{ij} \tag{16}$$

where ξ and η are the parametric coordinates. The rational basis functions R are evaluated based on a set of weights w_{ij} associated to each control point and B-Spline basis functions N defined for each parametric variable:

$$R_{ij}(\xi, \eta) = \frac{N_{i,p}(\xi) \, N_{j,q}(\eta) \, w_{ij}}{W(\xi, \eta)} \tag{17}$$

where W is the bivariate weight function expressed as:

$$W(\xi, \eta) = \sum_{\hat{i}=1}^{n} \sum_{\hat{j}=1}^{m} N_{\hat{i},p}(\xi) \, N_{\hat{j},q}(\eta) \, w_{\hat{i}\hat{j}} \tag{18}$$

A NURBS surface with its mesh of control points is shown in Fig. 3.

The definition of $N_{i,p}$ basis requires a knot vector, composed by non-negative and non-decreasing parametric values bounded by the parametric interval in which the surface is defined. It is important to note that one knot vector is required for each parametric variable of the surface. Given a knot vector $\Xi = [\xi_1, \xi_2, ..., \xi_{n+p+1}]$, the B-Spline basis functions are evaluated by the recursive Cox-de Boor formula [19]:

$$N_{i,0}(\xi) = \begin{cases} 1, & \xi_i \le \xi < \xi_{i+1} \\ 0, & \text{otherwise} \end{cases} \tag{19}$$

$$N_{i,p}(\xi) = \frac{\xi - \xi_i}{\xi_{i+p} - \xi_i} N_{i,p-1}(\xi) + \frac{\xi_{i+p+1} - \xi}{\xi_{i+p+1} - \xi_{i+1}} N_{i+1,p-1}(\xi) \tag{20}$$

The number of basis functions n can be evaluated based in the knot vector size ks and the degree p by:

$$n = ks - p - 1 \tag{21}$$

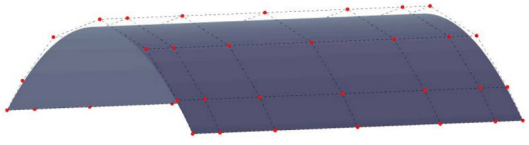

Fig. 3. NURBS surface and its control mesh.

NURBS basis functions inherits important properties from B-Spline basis functions [19]:

- Non-negativity, since $N_{i,p}(\xi) \geq 0$;
- Linear independence;
- Partition of unity ($\sum_{i=1}^{n} N_{i,p}(\xi) = 1$);
- Compact support, since the basis $N_{i,p}$ are zero for parametric values outside the knot interval $[\xi_i, \xi_{n+p+i}]$;
- The basis $N_{i,p}$ has continuity C^{p-k} at the knots, where k is the knot multiplicity.

The partial derivatives of NURBS basis functions showed in Equation (17) can be evaluated using the quotient rule:

$$R_{ij,\xi} = w_{ij}\, N_{j,q}(\eta)\, \frac{W\, N_{i,p}{}'(\xi) - W_{,\xi}\, N_{i,p}(\xi)}{W^2}$$
$$R_{ij,\eta} = w_{ij}\, N_{i,p}(\xi)\, \frac{W\, N_{j,q}{}'(\eta) - W_{,\eta}\, N_{j,q}(\eta)}{W^2} \tag{22}$$

where the derivatives of B-Spline basis functions are given by

$$N_{i,p}{}' = \frac{p}{\xi_{i+p} - \xi_i} N_{i,p-1}(\xi) - \frac{p}{\xi_{i+p+1} - \xi_{i+1}} N_{i+1,p-1}(\xi) \tag{23}$$

The derivatives of NURBS basis functions are used in the evaluation of the stiffness matrix of the isogeometric element presented in the following.

It is important to note that there are efficient algorithms to modify the description of a NURBS surface without modifying its shape [19]. The Knot Insertion algorithm adds one new knot ξ_i in the knot vector, as well as new basis functions and new control points to the NURBS surface. The Degree Elevation algorithm increases the degree of a NURBS keeping its current continuity between the knot spans. These algorithms can be used to refine the numerical model without modifying the shell geometry and are equivalent to the h and p refinements used in FEM, respectively. The k-refinement is obtained by combining both algorithms, increasing the continuity between isogeometric elements within the same patch [10]. Fig. 4 illustrates B-Spline basis functions obtained by k-refinement.

3.2. Element formulation

In this work, the geometry of a shallow shell is described by a NURBS surface given by:

$$x = \sum_{k=1}^{nn} R_k\, x_k; \quad y = \sum_{k=1}^{nn} R_k\, y_k; \quad z = \sum_{k=1}^{nn} R_k\, z_{0k} \tag{24}$$

where R_k are the functions defined by Equation (17) and nn is the number of control points of the surface ($nn = n \times m$). It is important to note that a single index k is used to identify the control points and bivariate bases. Such index is related to the indices i and j of the bivariate bases as $k = (j-1)n + i$.

The concept of an isogeometric element can be associated with each knot span of a NURBS patch [11]. The property of compact support of NURBS basis functions allows associating the degrees of freedom of each element with the control points whose base functions are non-zero at the corresponding knot span. Thus, the integrations required to compute the internal forces and stiffness matrix can be carried out in an element-wise fashion. The global vectors and matrices are assembled summing up the element contributions, exactly as in FEM.

In the isogeometric analysis of shallow shells, the in-plane and transverse displacements (u, v and w, respectively) and rotations (θ_x and θ_y) at the element mid-surface are approximated from the element degrees of freedom at control points as:

$$u = \sum_{k=1}^{nn} R_k\, u_k; \quad v = \sum_{k=1}^{nn} R_k\, v_k; \quad w = \sum_{k=1}^{nn} R_k\, w_k;$$
$$\theta_x = \sum_{k=1}^{nn} R_k\, \theta_{xk}; \quad \theta_y = \sum_{k=1}^{nn} R_k\, \theta_{yk} \tag{25}$$

This equation can be written in matrix format as

$$\mathbf{u} = \mathbf{R}\, \mathbf{u}_e \tag{26}$$

where $\mathbf{u}$ and $\mathbf{u}_e$ are the vectors of displacements of the shell mid-surface and its control points, respectively, and $\mathbf{R}$ is the matrix of shape functions, given by:

$$\mathbf{R} = [\mathbf{R}_1 \;\; \mathbf{R}_2 \;\; \ldots \;\; \mathbf{R}_{nn}] \tag{27}$$

The sub-matrix associated with each control point is

$$\mathbf{R}_k = R_k\, \mathbf{I}_{5\times 5} \tag{28}$$

where $\mathbf{I}$ is the identity matrix.

The generalized shell strains can be written as:

$$\hat{\varepsilon} = \begin{Bmatrix} \varepsilon^m \\ \kappa \\ \gamma \end{Bmatrix} = \begin{Bmatrix} \varepsilon_0^m \\ \kappa \\ \gamma \end{Bmatrix} + \begin{Bmatrix} \varepsilon_L^m \\ 0 \\ 0 \end{Bmatrix} \tag{29}$$

These strains are related to the element degrees of freedom:

$$\hat{\varepsilon} = \begin{bmatrix} \mathbf{B}_0^m \\ \mathbf{B}_0^b \\ \mathbf{B}_0^s \end{bmatrix} \mathbf{u}_e + \frac{1}{2} \begin{bmatrix} \mathbf{B}_L^m \\ 0 \\ 0 \end{bmatrix} \mathbf{u}_e = \left(\mathbf{B}_0 + \frac{1}{2}\, \mathbf{B}_L \right) \mathbf{u}_e \tag{30}$$

Using Equations (2), (4), (5) and (25))-(28), the sub-matrices of for each control point are given by:

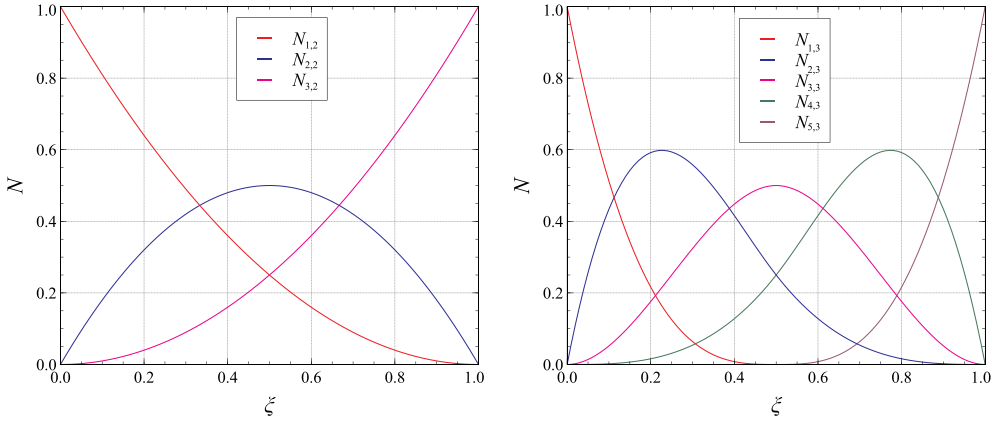

(a) $p = 2$ and $\Xi = [0, 0, 0, 1, 1, 1]$. (b) $p = 3$ and $\Xi = [0, 0, 0, 0, 0.5, 1, 1, 1, 1]$.

Fig. 4. B-Spline basis functions.

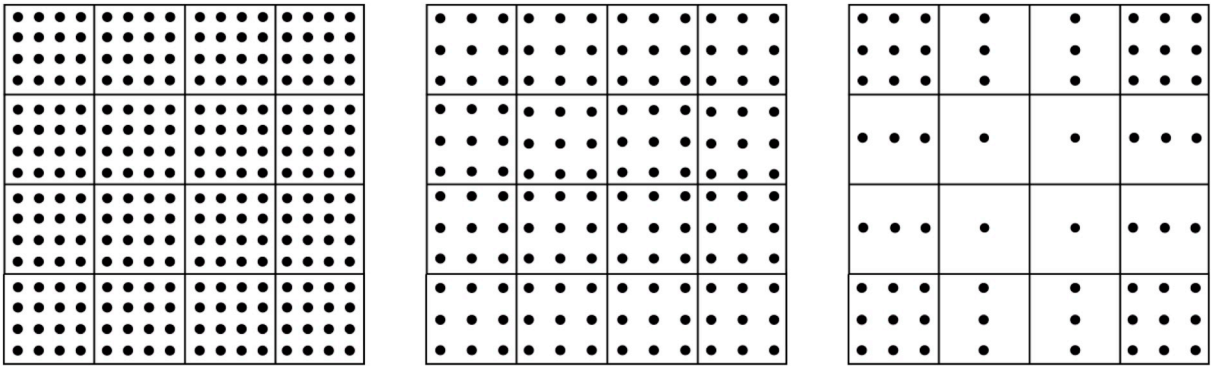

Fig. 5. Gauss integration for cubic NURBS.

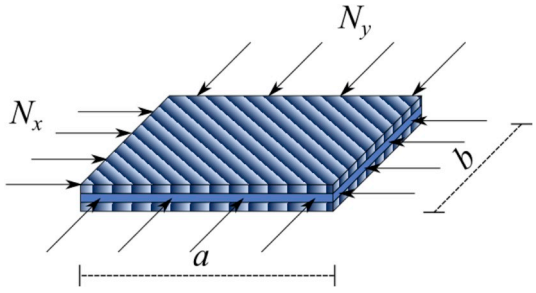

Fig. 6. Square plate subjected to biaxial compression.

$$\mathbf{B}_0^m = \begin{bmatrix} R_{k,x} & 0 & Z_x\, R_{k,x} & 0 & 0 \\ 0 & R_{k,y} & Z_y\, R_{k,y} & 0 & 0 \\ R_{k,y} & R_{k,x} & Z_x\, R_{k,y} + Z_y\, R_{k,x} & 0 & 0 \end{bmatrix}$$

$$\mathbf{B}_0^b = \begin{bmatrix} 0 & 0 & 0 & 0 & R_{k,x} \\ 0 & 0 & 0 & -R_{k,y} & 0 \\ 0 & 0 & 0 & -R_{k,x} & R_{k,y} \end{bmatrix}$$

$$\mathbf{B}_0^s = \begin{bmatrix} 0 & 0 & R_{k,x} & 0 & R_k \\ 0 & 0 & R_{k,y} & -R_k & 0 \end{bmatrix}$$

$$\mathbf{B}_L^m = \begin{bmatrix} 0 & 0 & W_x\, R_{k,x} & 0 & 0 \\ 0 & 0 & W_y\, R_{k,y} & 0 & 0 \\ 0 & 0 & W_x\, R_{k,y} + W_y\, R_{k,x} & 0 & 0 \end{bmatrix} \tag{31}$$

Where

$$Z_x = \sum_{k=1}^{nn} R_{k,x}\, z_{0k}; \quad Z_y = \sum_{k=1}^{nn} R_{k,y}\, z_{0k};$$
$$W_x = \sum_{k=1}^{nn} R_{k,x}\, w_k; \quad W_y = \sum_{k=1}^{nn} R_{k,y}\, w_k; \tag{32}$$

3.3. Nonlinear analysis

The internal force vector $\mathbf{g}$ is obtained from the Principle of Virtual Work:

$$\mathbf{g}(\mathbf{u}) = \int_{A_0} \bar{\mathbf{B}}^T\, \hat{\boldsymbol{\sigma}}\, dA_0 \tag{33}$$

where $\bar{\mathbf{B}} = \mathbf{B}_0 + \mathbf{B}_L$ relates the variation of the generalized strains with the variation of displacements ($\delta\hat{\boldsymbol{\varepsilon}} = \bar{\mathbf{B}}\, \delta\mathbf{u}_e$). The integration is carried out at the original element mid-surface, since the element is based on the Total Lagrangian (TL) approach.

The equilibrium equations of the isogeometric model for displacement independent loads can be written as

$$\mathbf{r}(\mathbf{u}, \lambda) = \mathbf{g}(\mathbf{u}) - \lambda\, \mathbf{f} \tag{34}$$

where $\mathbf{r}$ is the residual vector, $\mathbf{u}$ is the vector of degrees of freedom, $\mathbf{g}$ is the internal force vector, λ is the load factor, and $\mathbf{f}$ is the reference load vector. The load-displacement curve can be obtained using appropriate incremental-iterative algorithms, as the arc-length method [40].

Table 1
Composite material properties.

E_1/E_2	G_{12}/E_2	ν_{12}	G_{12}/G_{13}	G_{23}/E_2
25	0.5	0.25	1	0.2

These incremental-iterative algorithms are based on Newton-Raphson iterations, requiring the computation of the tangent stiffness matrix ($\mathbf{K}_T$):

$$\mathbf{K}_T = \frac{\partial \mathbf{g}}{\partial \mathbf{u}} = \mathbf{K}_L + \mathbf{K}_\sigma \tag{35}$$

where material stiffness matrix $\mathbf{K}_L$ and the geometric stiffness matrix $\mathbf{K}_\sigma$ are given by:

$$\mathbf{K}_L = \int_{A_0} \bar{\mathbf{B}}^T\, \frac{\partial \hat{\boldsymbol{\sigma}}}{\partial \mathbf{u}}\, dA_0 = \int_{A_0} \bar{\mathbf{B}}^T\, \mathbf{C}_T\, \bar{\mathbf{B}}\, dA_0 \tag{36}$$

$$\mathbf{K}_\sigma = \int_{A_0} \frac{\partial \bar{\mathbf{B}}^T}{\partial \mathbf{u}}\, \boldsymbol{\sigma}\, dA_0 = \int_{A_0} \mathbf{G}^T\, \mathbf{S}\, \mathbf{G}\, dA_0 \tag{37}$$

where $\mathbf{C}_T$ is the tangent constitutive matrix ($\mathrm{d}\hat{\boldsymbol{\sigma}} = \mathbf{C}_T\, d\hat{\boldsymbol{\varepsilon}}$) and

$$\mathbf{G} = \begin{bmatrix} 0 & 0 & R_{k,x} & 0 & 0 \\ 0 & 0 & R_{k,y} & 0 & 0 \end{bmatrix}$$
$$\mathbf{S} = \begin{bmatrix} N_x & N_{xy} \\ N_{xy} & N_y \end{bmatrix} \tag{38}$$

The arc-length method and other path-following methods can trace the equilibrium paths presenting complex nonlinear behavior (e.g. snap-through, snap-back and loops), but can only trace the fundamental (primary) path of structures with bifurcation buckling. It is worth noting that the study of the post-critical behavior of thin-walled structures is very important since it allows classifying the stability loss, determining the structure load capacity and quantifying its sensitivity to initial imperfections. Therefore, numerical approaches to stability analysis require the evaluation of critical points and the determination of post-critical paths [41–43].

The tangent stiffness matrix is singular at critical (limit and bifurcation) points. Therefore:

$$\det \mathbf{K}(\mathbf{u}, \lambda) = 0 \tag{39}$$

Alternatively, the critical point can be detected using the zero eigenvalue condition:

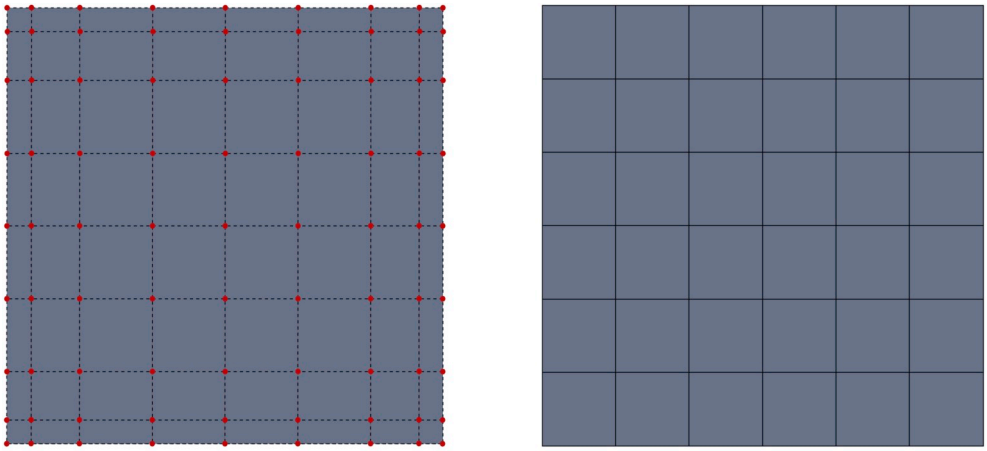

(a) Control points. (b) Elements.

Fig. 7. Isogeometric model ($p = 3$).

Table 2
Buckling loads ($\lambda = N_{cr}\, a^2/\pi^2\, D$) for isotropic plates.

Mesh	Full	Dif (%)	R_{FEM}	Dif (%)	R_{IGA}	Dif (%)
4 × 4	4.4265	10.66	4.4077	10.19	3.9820	−0.45
6 × 6	4.2492	6.23	4.2041	5.10	3.9942	−0.14
8 × 8	4.0780	1.95	4.0575	1.44	3.9975	−0.06
10 × 10	4.0227	0.57	4.0161	0.40	3.9984	−0.04
[50]	4.0000					

Table 3
Buckling loads ($\lambda = N_{cr}\, a^2/E_2\, h^3$) for cross-ply plates $(0/90)_s$.

Mesh	Full	Dif (%)	R_{FEM}	Dif (%)	R_{IGA}	Dif (%)
4 × 4	12.779	8.79	12.526	6.63	12.010	2.24
6 × 6	11.937	1.62	11.883	1.15	11.851	0.89
8 × 8	11.784	0.31	11.774	0.23	11.795	0.41
10 × 10	11.757	0.08	11.754	0.06	11.772	0.21
[39]	11.747					

Table 4
Buckling loads ($\lambda = N_{cr}\, a^2/E_2\, h^3$) for angle-ply plates $(45/\text{-}45)_s$.

Mesh	Full	Dif (%)	R_{FEM}	Dif (%)	R_{IGA}	Dif (%)
4 × 4	18.767	18.19	18.213	14.70	16.469	3.72
6 × 6	16.710	5.24	16.538	4.15	16.107	1.44
8 × 8	16.195	1.99	16.142	1.66	15.987	0.68
10 × 10	16.033	0.98	16.008	0.82	15.913	0.22
[39]	15.878					

$$\mathbf{K}(\mathbf{u}, \lambda)\, \boldsymbol{\varphi} = 0, \quad \text{with } \boldsymbol{\varphi} = 1 \tag{40}$$

where $\boldsymbol{\varphi}$ is the associated eigenvector, which represents the buckling mode. Therefore, the critical point $(\mathbf{u}_{cr}, \lambda_{cr})$ along the equilibrium path can be determined as the solution of the nonlinear system

$$\begin{bmatrix} \mathbf{r}(\mathbf{u}, \lambda) \\ \mathbf{K}(\mathbf{u}, \lambda)\, \boldsymbol{\varphi} \\ ||\boldsymbol{\varphi}|| - 1 \end{bmatrix} = 0 \tag{41}$$

Numerical procedures have been proposed to efficiently solve this system [41–43]. After the critical point computation, the bucking mode can be used for its classification [43]:

$$\begin{cases} \boldsymbol{\phi}^T\, \mathbf{f} \neq 0 \Rightarrow \text{limit point} \\ \boldsymbol{\phi}^T\, \mathbf{f} = 0 \Rightarrow \text{bifurcation point} \end{cases} \tag{42}$$

Finally, the buckling mode can be used to perform the branch-switching [43] to the post-critical path at a bifurcation point. It is important to note that this approach can be used to study the stability of perfect and imperfect structures, with both bifurcation and limit point instabilities.

3.4. Numerical integration

The isogeometric formulation presented in this work can be used considering linear or nonlinear constitutive models. In the case of materials with linear behavior, the constitutive matrices ($\mathbf{Q}_m$ and $\mathbf{Q}_s$) of each ply is constant, as well as the laminate constitutive matrix ($\mathbf{C}_T = \mathbf{C}$). In this case, the $\mathbf{C}$ matrix can be computed exactly from the $\mathbf{A}$, $\mathbf{B}$, $\mathbf{D}$, and $\mathbf{G}$ matrices presented in Equations (14) and (15). Therefore, the numerical integration is performed only on the element mid-surface using the Gaussian quadrature. The full integration of the element stiffness matrix requires $p + 1$ integration points for each parametric coordinate, due to the presence of basis functions R_k of degree p in matrix $\mathbf{B}_0^s$, as shown in Equation (31).

It is important to note that IGA cannot avoid the shear locking that degrades the convergence of fully integrated Reissner-Mindlin elements [34], especially for thin-walled plates and shells and low order approximations. According to Ref. [44], locking is present independent of the order of the adopted polynomial and Reissner-Mindlin shell elements undergo membrane and transverse shear locking. This occurs due to the field inconsistency of the adopted displacement interpolation, which does not depend on the order of the displacement approximation. Therefore, the use of higher order displacement approximations reduces but does not eliminate locking.

An alternative to avoid shear locking is to use the third-order shear deformation theory (TSDT) [39] instead of the FSDT (Reissner-Mindlin theory). However, TSDT is less efficient that FSDT, since it requires the evaluation of additional sectional forces and matrices [39]. It is also more complex since it requires C^1 continuity, which leads to difficulties for structures with multiple NURBS patches. On the other hand, the proposed formulation based on FSDT requires only C^0 continuity, simplifying the analysis of complex structures with multiple patches. In addition, the differences in displacements and buckling loads obtained using TSDT and FSDT for thin-walled composite structures are negligible [39]. It is also important to note that curved shell elements suffer not only shear locking but also membrane locking [35].

According to Ref. [45], several techniques are used to alleviate the locking problem, as Uniform Reduced Integration and Selective Reduced Integration [37], $\bar{B}$ method [46] and Discrete Shear Gap [17,34] approach. In the uniform reduced integration the bending and shear stiffness matrices are integrated using the same number of Gauss points, while the selective integration adopts a different number of points for

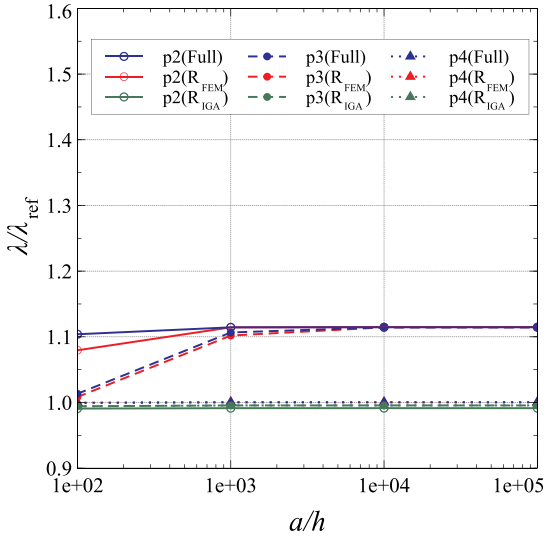

(a) Isotropic.

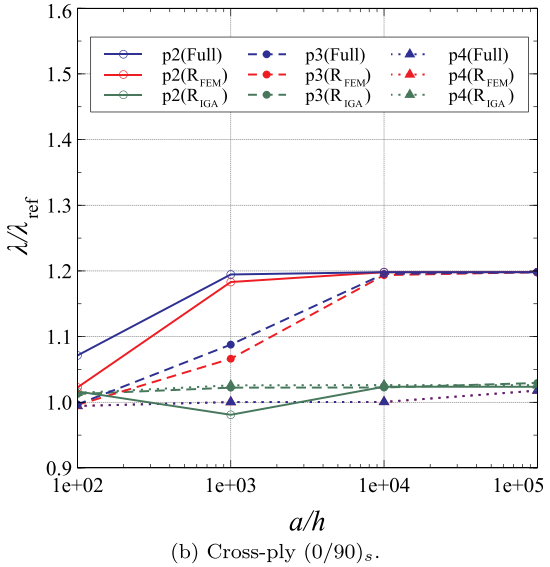

(b) Cross-ply $(0/90)_s$.

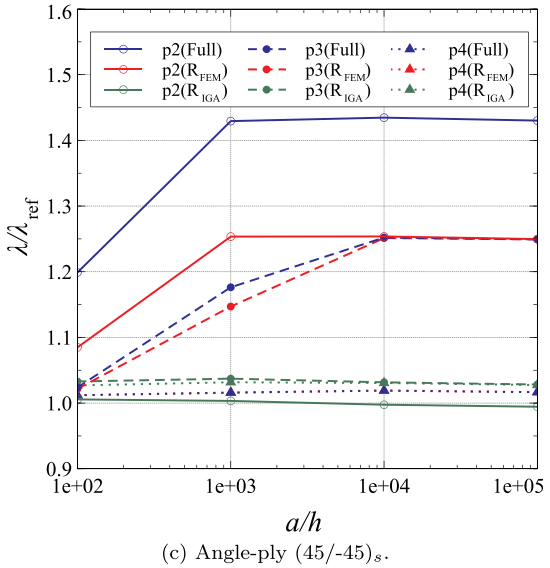

(c) Angle-ply $(45/-45)_s$.

Fig. 8. Buckling loads for *k*-refinement.

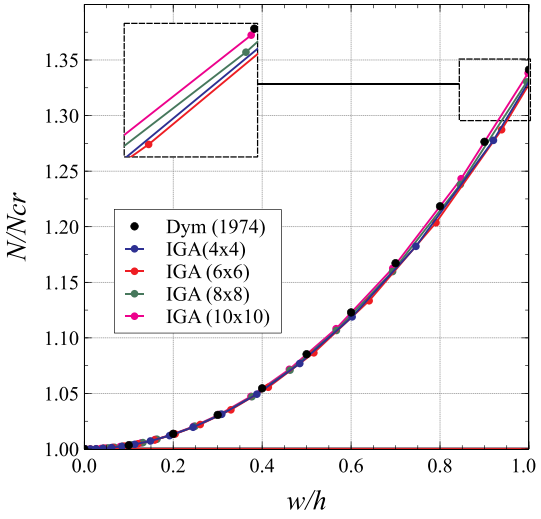

(a) Isotropic.

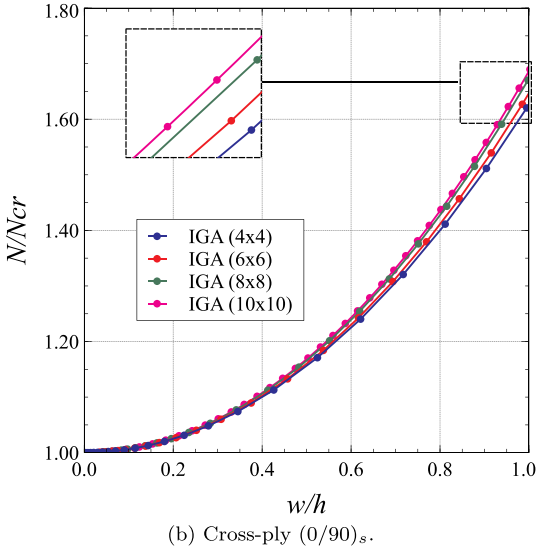

(b) Cross-ply $(0/90)_s$.

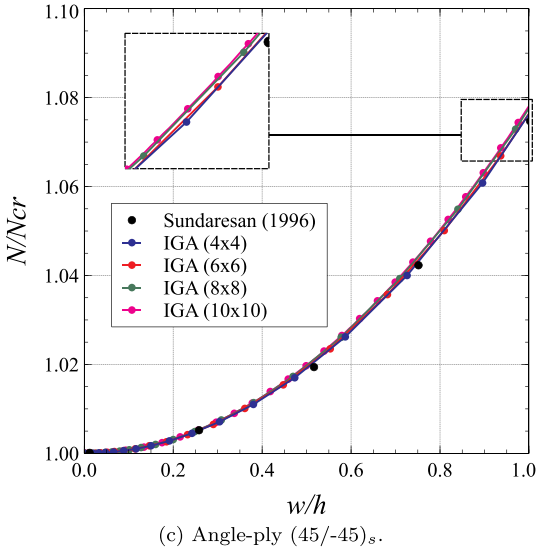

(c) Angle-ply $(45/-45)_s$.

Fig. 9. Post-critical behavior of perfect plates with $p = 3$ and *h*-refinement.

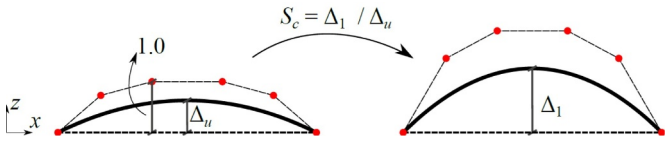

Fig. 10. Application of an initial imperfection in plates.

each matrix, leading to a more complex computational implementation.

It is well known that the uniform reduced integration scheme (R_{FEM}) using p integration points for each parametric coordinate does alleviate, but not eliminates, locking of Reissner-Mindlin elements in FEM while also generating spurious (or hourglass) modes. On the other hand [37], presented a uniform reduced integration scheme (R_{IGA}) that eliminates shear and membrane locking, without generating spurious modes, in NURBS based isogeometric analysis of plates and shells with small strains. Owing to the high regularity of NURBS basis functions with C^{p-1} continuity obtained through k-refinement, this approach increases simultaneously the accuracy and computational efficiency of IGA formulation. In this work the accuracy of Full, R_{FEM} and R_{IGA} integration schemes will be assessed in the buckling and geometrically nonlinear analysis of plates and shells. These integration schemes are illustrated in Fig. 5 for $p = 3$.

It is interesting to note that an IGA discretization generated by k-refinement uses fewer degrees of freedom (DOF) than a finite element model with the same number of elements and basis degree (p). Since the reduced integration scheme (R_{IGA}) requires less Gauss points than the finite element method (R_{FEM}), this isogeometric approach is computationally more efficient than FEM with C^0 elements.

4. Numerical examples

The formulation presented in this work was implemented in FAST (Finite element AnalySis Tool), which is a structural analysis program implemented in C++ programming language using object-oriented programming (OOP) techniques. FAST was initially developed to perform finite element analysis of structures with homogeneous and composite materials. Recently, the software was extended with the implementation of NURBS-based isogeometric analysis using the Bézier extraction approach [13]. This software was used in the numerical analysis presented in the following. The results obtained using IGA/FAST will be compared with results available in the literature and results obtained using the quadratic Reissner-Mindlin shell element with reduced integration (S8R) of software ABAQUS [47].

4.1. Stability analysis of simply supported plates

This example deals with the study of buckling and post-buckling behavior of simply supported square plates, isotropic and laminated, subjected to uniaxial or biaxial compression, as shown in Fig. 6. The elastic properties of the composite material are presented in Table 1.

The boundary conditions used by Refs. [48,49] were adopted here:

$$\begin{cases} \text{At } x = 0,\ u = w = \theta_x = 0 \\ \text{At } y = 0,\ v = w = \theta_y = 0 \\ \text{At } x = a,\ u = \text{constant and } w = \theta_x = 0 \\ \text{At } y = b,\ v = \text{constant and } w = \theta_y = 0 \end{cases} \tag{43}$$

An isogeometric model of the laminated plate with 6×6 cubic elements is shown in Fig. 7. It is interesting to note that, unlike FE nodes, NURBS control points are not necessarily located at the element boundaries.

Initially, a convergence study of the proposed formulation was

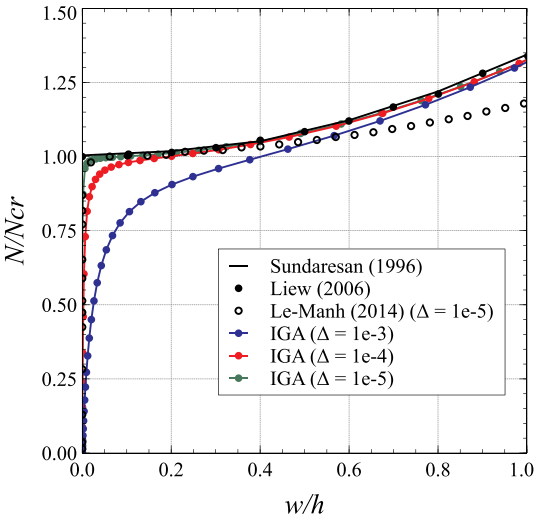

(a) Isotropic.

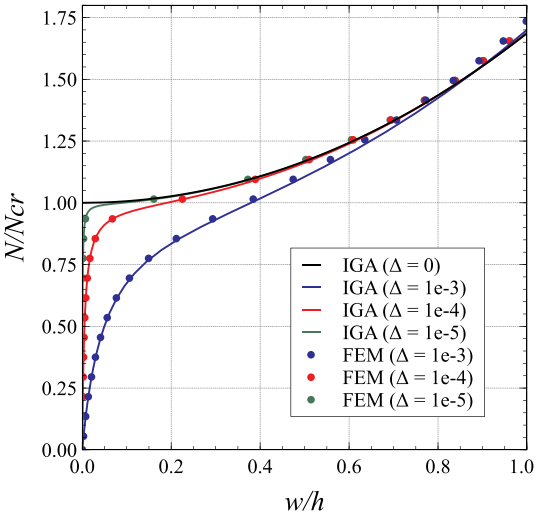

(b) Cross-ply $(0/90)_s$.

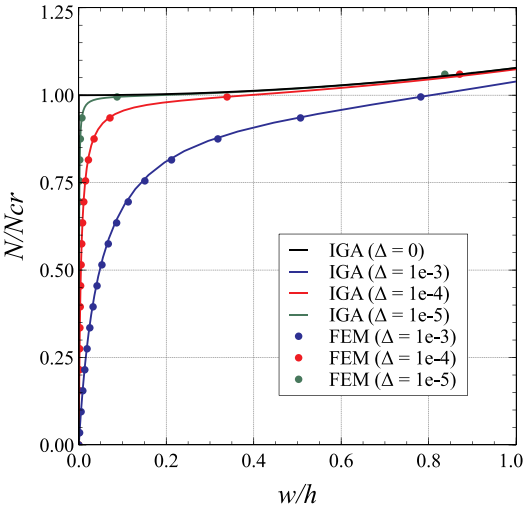

(c) Angle-ply $(45/-45)_s$.

Fig. 11. Nonlinear behavior of imperfect plates.

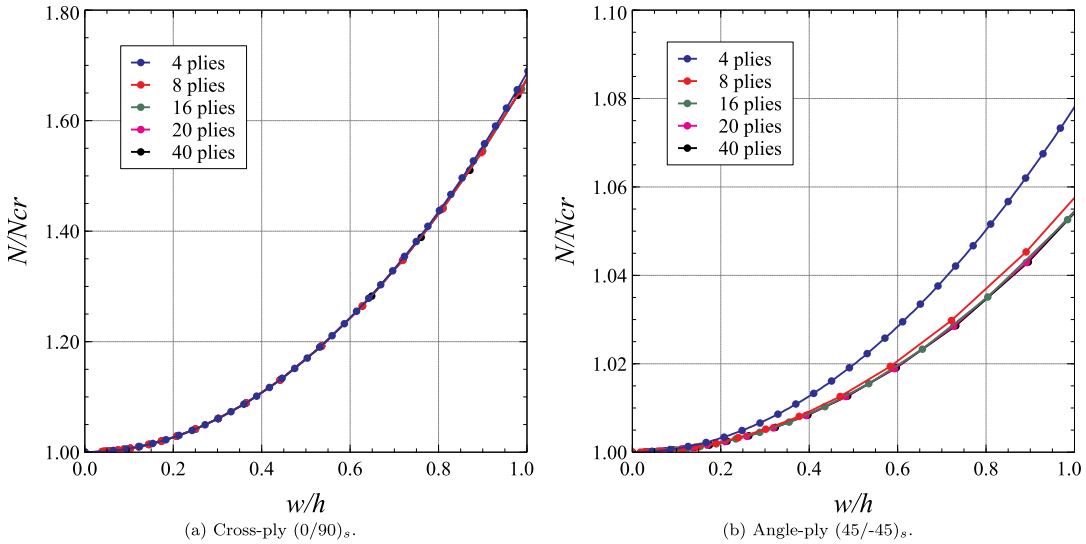

Fig. 12. Effect of the number of plies.

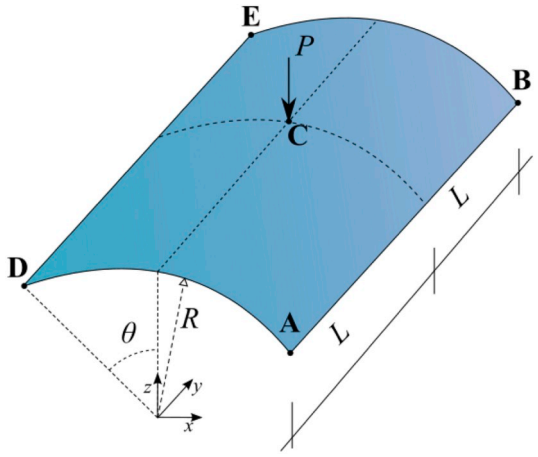

Fig. 13. Shallow shell subjected to a concentrated load.

Table 5
Composite material properties.

E_1	E_2	ν_{12}	$G_{12} = G_{13}$	G_{23}
3300	1100	0.25	660	440

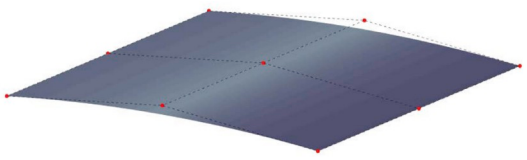

Fig. 14. Initial quadratic model for *k*-refinement with 9 control points and 1 element.

carried out for the classical linearized buckling (eigenvalue) analysis, considering different meshes, basis functions degrees, layups, and integration schemes. It is important to note that the isotropic plates are subjected to uniaxial loading and the laminated plates are subjected to biaxial loading. The reference buckling loads for isotropic plates are computed using the analytical solution for Kirchhoff theory [50], for cross-ply plates are computed using the analytical solution for the Classical Lamination Theory [39] and for angle-ply plates are computed using FEM with a very fine mesh (40 × 40). The layups adopted for cross-ply and angle-ply plates are $(0/90)_s$ and $(45/-45)_s$, respectively.

Table 2, Table 3, and Table 4 present the buckling loads of thin-walled isotropic, cross-ply and angle-ply square plates with $a/h = 1000$, respectively, evaluated using IGA with cubic basis functions ($p = 3$). The results show that the proposed formulation converges to the reference values with mesh discretization for all layups and integration schemes. It is interesting to note that convergence is faster for isotropic than laminated plates. Moreover, the couplings present in the **D** matrix of angle-ply laminates degrade the accuracy with respect to cross-ply laminates. Finally, the results show that the accuracy of R_{IGA} is clearly superior to the other options, leading to excellent results even for coarse meshes.

Fig. 8 presents the results obtained using IGA models generated with *k*-refinement and C^{p-1} continuity. A fixed 4 × 4 mesh is used in all analysis while the a/h ratio is varied. The accuracy of solutions obtained using Full and $\mathrm{R_{FEM}}$ integrations clearly degrades when thickness decreases, especially for quadratic and cubic elements, due to shear locking. As occurs for the *h*-refinement, shear locking is smaller for isotropic plates, intermediate for cross-ply plates and worse for angle-ply plates.

As expected, the shear locking decreases for high order elements. Thus, fourth order elements generate excellent results for all integration schemes for the entire range of a/h considered here, which includes very thin plates.

Finally, the results show that the $\mathrm{R_{IGA}}$ integration eliminates shear locking, since its accuracy is independent of the a/h ratio. It can be noted that excellent results are obtained even for quadratic approximation. Since $\mathrm{R_{IGA}}$ is not only more accurate, but also more efficient than the other integration schemes, it will be used in the nonlinear analyses presented in the following.

The geometrically nonlinear analysis of isotropic and laminated plates was carried out and the results are presented in the following. The plates have $a/h = 100$, except for only one example with an isotropic plate where the ratio is $a/h = 50$, since these are the same ratios used by Refs. [21,48]. Fig. 9 presents the post-buckling equilibrium paths of perfect plates obtained using cubic isogeometric meshes and *h*-refinement. It is worth noting that very good results were obtained even for the coarsest mesh (4 × 4). Comparison with the analytical post-buckling solution for thin isotropic plates [50] shows the convergence of the isogeometric solution under *h*-refinement. In addition, isogeometric results for angle-ply plates are in good agreement with [48] and the small differences are due to the very coarse mesh used in their FEM solution. For all layups, the convergence is from below, with stiffer post-buckling responses obtained for more refined meshes.

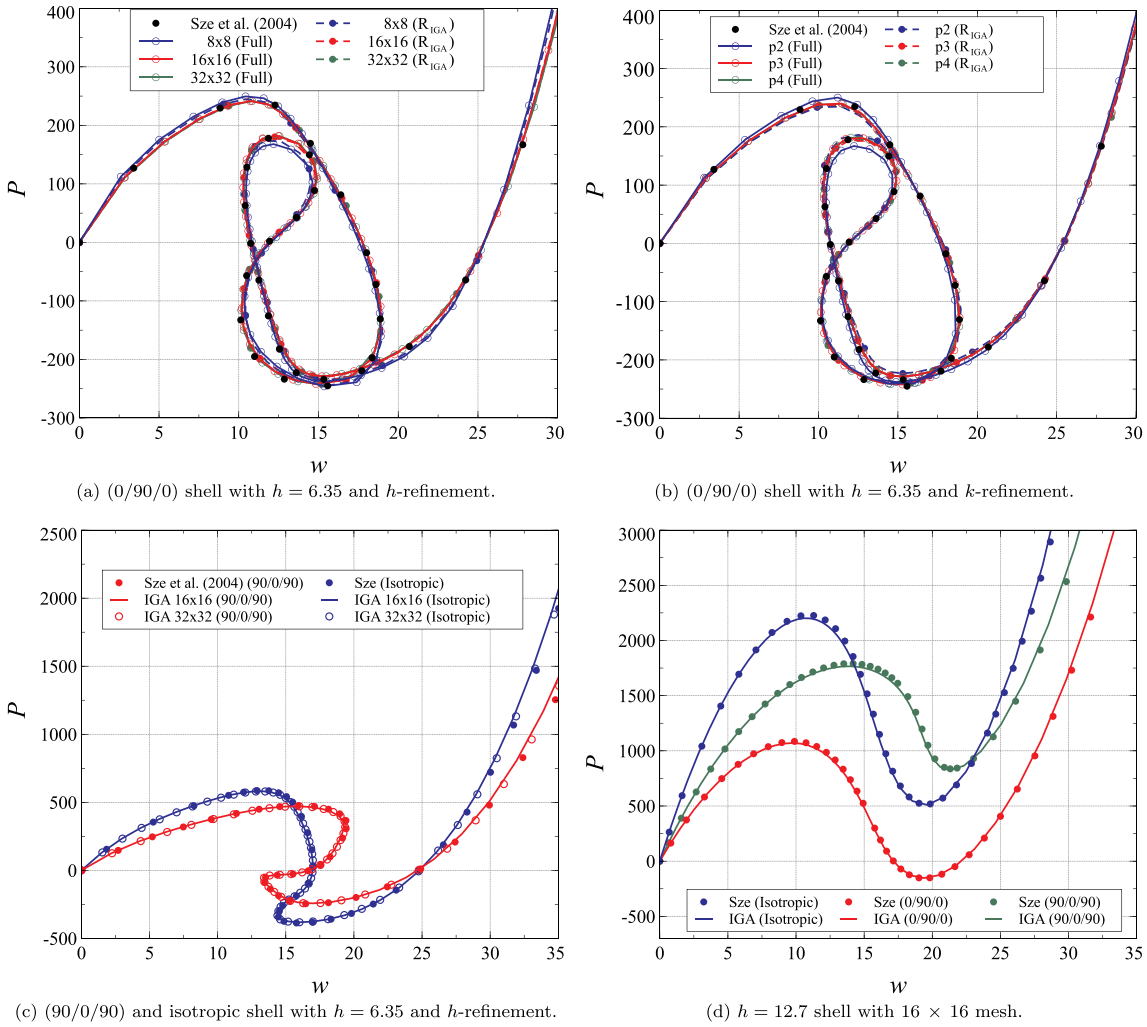

(a) (0/90/0) shell with $h = 6.35$ and h-refinement.

(b) (0/90/0) shell with $h = 6.35$ and k-refinement.

(c) (90/0/90) and isotropic shell with $h = 6.35$ and h-refinement.

(d) $h = 12.7$ shell with 16×16 mesh.

Fig. 15. Load-deflection curves of the cylindrical roof.

It is interesting to note that, while the critical loads of angle-ply plates are higher than the cross-ply ones, the opposite occurs for the post-critical strength reserve, since the N/N_{cr} ratio of cross-ply plates present a much smaller increase with the transverse displacements (w/h). However, all laminates present a stable symmetrical post-critical behavior.

In order to study the imperfection sensitivity, the geometry of imperfect structures can be modeled as a linear combination of their buckling modes (φ_i):

$$\mathbf{x}_{imp} = \mathbf{x}_{perf} + \sum_{i=1}^{n} \Delta_i \, \varphi_i \tag{44}$$

where $\mathbf{x}_{imp}$ and $\mathbf{x}_{perf}$ are the coordinates of the points that define the geometry in the imperfect and perfect configuration, respectively, and Δ_i is the amplitude of imperfection related to the buckling mode φ_i, whose largest component has a unit value. In this work, only the first buckling mode will be used to describe the geometric imperfection.

It is worth noting that, contrary to FEM nodes, the isogeometric control points do not interpolate the geometric model. Thus, an imperfect geometry with specific amplitude cannot be obtained directly by the application of Equation (44). However, as NURBS have the affine invariance property [19], the geometry with the correct imperfection amplitude can be obtained by applying a scale transformation $S_c = \Delta_1/\Delta_u$ in z-coordinates of the plate control points. Fig. 10 illustrates this procedure.

A 10×10 mesh of cubic C^2 elements is used to study the imperfection sensitivity, except for the square isotropic plate with $a/h = 50$, where a 6×6 mesh is used for comparison with the results obtained by Ref. [21]. It is important to note that the boundary conditions for in-plane displacements (u, v) are not specified in Ref. [21].

The IGA results are compared with FEM results obtained using a 40×40 mesh of S8R shell elements and other results available in the literature. The curves presented in Fig. 11 show that the proposed shallow shell isogeometric formulation leads to very accurate results in the nonlinear analysis of imperfect plates when compared with FEM and reference solutions. On the other hand, there is a clear difference of the results presented by Ref. [21] with respect to the other results. This difference was erroneously attributed to certain characteristics of the IGA approach [21]. However, as the IGA formulation proposed in the present work lead to very accurate results, the differences in the results obtained by Ref. [21] are probably due to the use of different boundary conditions for in-plane displacements.

The results show that the cross-ply plates have a higher post-critical stiffness than isotropic and angle-ply plates. In fact, the results show that plates with angle-ply layups present a negligible post-critical strength increase. It is interesting to that laminate plates, as isotropic ones, are only mildly imperfection sensitive.

Finally, the proposed formulation was used to study the effect of the number of plies in the post-critical behavior. In this study, the number of plies was increased keeping constant the laminate thickness. According to Fig. 12, the increase in the number of plies does not influence the post-critical response of cross-ply plates, but further decreases the post-critical stiffness of angle-ply plates.

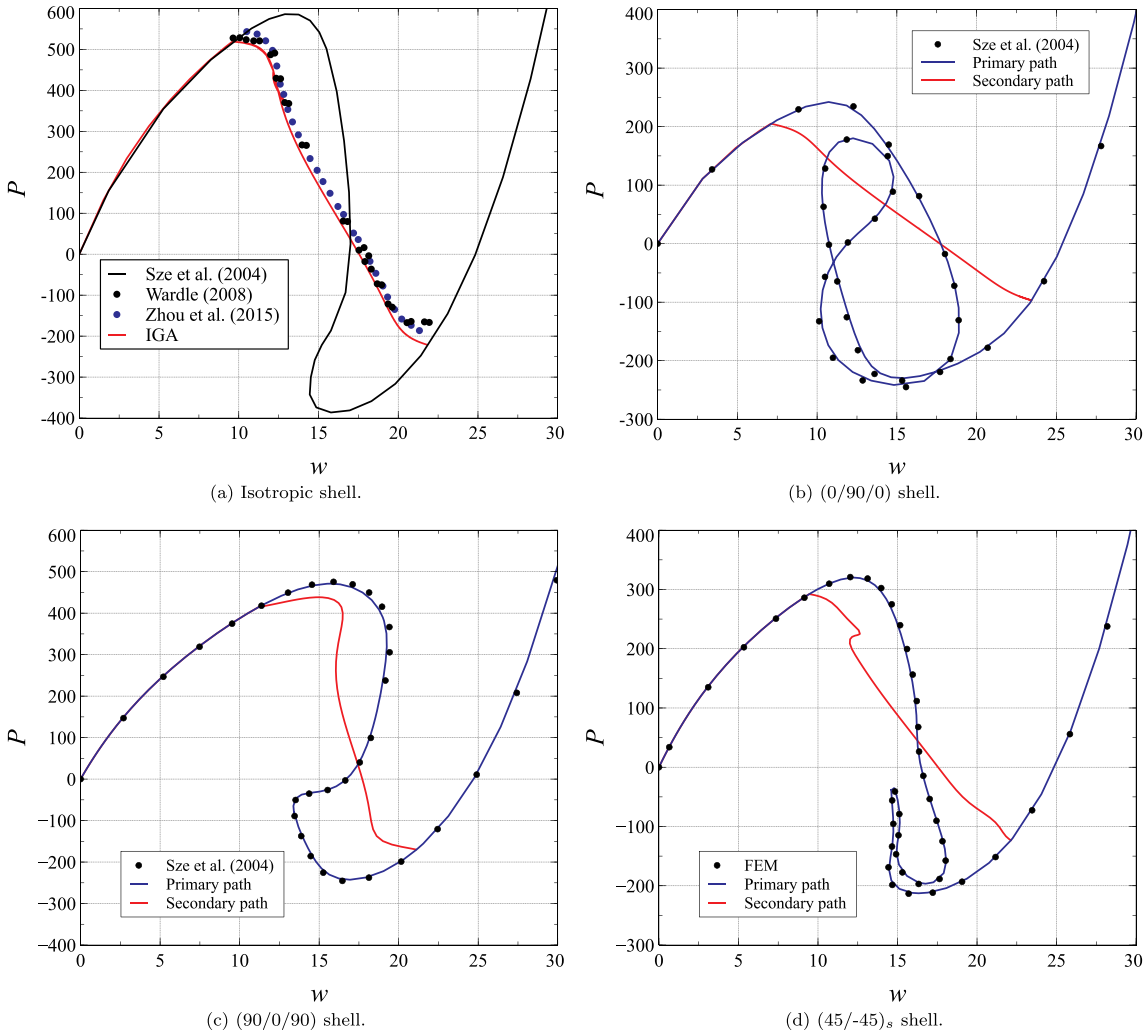

(a) Isotropic shell. (b) (0/90/0) shell. (c) (90/0/90) shell. (d) $(45/-45)_s$ shell.

Fig. 16. Primary and secondary paths of the cylindrical roof ($h = 6.35$).

4.2. Cylindrical roof

This example addresses the nonlinear analysis of a cylindrical shell subjected to a concentrated load, as shown in Fig. 13. This shell was analyzed by several authors, including [38]. The geometric parameters of the structure are $R = 2540$, $\theta = 0.1$ rad, and $L = 254$. The structure is simply supported ($u = w = 0$) in AB andDE and free in AD and BE. The isotropic material properties are $E = 3102.75$ and $\nu = 0.3$. The composite material properties are presented in Table 5. It is important to note that the fibers in the 0° direction are parallel to the y-axis.

The FEM solution considered the symmetry and only a quarter of structure was discretized [38]. This increases the computational efficiency, but excludes non-symmetric deformation modes from the structural analysis. On the other hand, the symmetry was not used here and the whole shell was modeled using IGA in order to allow the consideration of symmetric and non-symmetric deformation modes. All meshes are obtained by k-refinement over an initial quadratic model with 1 element and 9 control points (Fig. 14). Several analyses were carried out considering isotropic and laminated shells with $h = 6.35$ and $h = 12.7$ and the results are presented in Fig. 15.

Fig. 15a presents IGA results for cubic basis functions with 8×8, 16×16 and 32×32 meshes, while Fig. 15b presents results obtained using a 16×16 with quadratic, cubic and quartic IGA models. Both Full and Reduced (R_{IGA}) integrations were considered. The results with cubic and quartic elements and both integration schemes are almost identical to the results of [38]. On the other hand, the quadratic approximation with R_{IGA} yields better results than those with Full integration, due to the locking presented by the fully integrated IGA formulation with low order basis functions.

Fig. 15c and d used only cubic bases and R_{IGA} integration. Fig. 15c shows results for 16×16 and 32×32 meshes, where the difference is only perceptible for large downward displacements ($w > 30$). Fig. 15d presents the results obtained for thickness $h = 12.7$, which are very close to the results of [38].

Fig. 15 indicates that, unlike from the plates studied in the previous example, these cylindrical shells present a nonlinear behavior even for small loads and lose stability by limit point. The results show that the thinner shells present a complex nonlinear behavior with snap-through, snap-backs, and loops (Fig. 15a, b, and 15c). On the other hand, the thicker shells present a simpler nonlinear behavior characterized by snap-through buckling. Moreover, it can be noted that the composite layup has a strong influence on the structure load-carrying capacity and nonlinear behavior.

The load-displacement curves presented in Fig. 15 correspond to the classical solution of this well-known benchmark problem [38], whose isotropic version was initially proposed by Ref. [51]. These curves represent a complex nonlinear behavior with snap-through and snap-back, but no bifurcations. However [52], showed that the isotropic shell presents a bifurcation point at a load level below the first limit point. Thus, a lower-energy equilibrium path exists corresponding to a bifurcation into an asymmetric deformation mode.

The critical point evaluation and branch-switching procedure

discussed in Section 3.3 were applied to the isogeometric model (16×16 mesh with $p = 3$ and R_{IGA} integration) of the isotropic and composite cylindrical shell. The obtained results are presented in Fig. 16. A very good agreement was obtained with the finite element results presented by Refs. [52,53] for the isotropic shell (Fig. 16a), confirming that the load-carrying capacity of this shell is smaller than the first limit load of the classical benchmark solution.

Furthermore, the cross-ply shells (Fig. 16b and c) present a similar behavior with a bifurcation at a load level inferior to the first limit point. Therefore, the composite shells also present a smaller load-carrying capacity than the classical benchmark solution presented in the literature [38] and the benchmark solution should be extended to consider not only the primary equilibrium path, but also the post-buckling secondary path. The angle-ply shell (Fig. 16d) was not studied in Ref. [38], but the primary paths obtained by IGA and FEM are in very good agreement. This shell also presents a bifurcation load smaller than the first limit load. Finally, it is worth noting that the load-carrying capacity of the cylindrical roof depends on the composite layup, showing the importance of using optimization techniques in the design of composite shells.

5. Conclusion

This work presented a NURBS-based isogeometric formulation for geometric nonlinear analysis of laminated plates and shallow shells based on the Reissner-Mindlin and Marguerre theories. This approach allows the exact representation of curved geometries and an easy application of the *h*, *p* and *k* refinements. The proposed formulation was successfully used in the stability analysis of plates and shallow shells with complex nonlinear behavior. Both bifurcation and limit point instabilities of perfect and imperfect structures were addressed. A classical laminated shell-buckling benchmark was extended to include post-buckling secondary paths after bifurcation points. It is important to note that not only the primary paths but also the bifurcation loads and post-buckling paths are strongly dependent on the composite layup.

The formulation presents a faster convergence for cross-ply and isotropic laminates, requiring coarser meshes than angle-ply laminates. Angle-ply plates subjected to biaxial loading present a higher buckling load than cross-ply plates with the same thickness. On the other hand, cross-ply plates exhibit a much higher post-buckling stiffening than angle-ply plates, independent of the number of plies. The results also showed that the nonlinear behavior of composite shells is strongly influenced not only by the composite layup but also by the shell thickness.

The obtained results show that the use of higher order basis functions alleviates, but not eliminates, locking when the isogeometric approach is used in the stability and geometrically nonlinear analysis of thin-walled plates and shells. However, locking can be easily eliminated using the appropriate reduced integration scheme for NURBS-based IGA approach. Finally, it is important to note that the use of this reduced integration scheme improves not only the accuracy but also the computational efficiency of the proposed formulation.

Acknowledgments

This study was financed in part by the Coordenação de Aperfeiçoamento de Pessoal de Nível Superior - Brasil (CAPES) - Finance Code 001 and Conselho Nacional de Desenvolvimento Científico e Tecnológico (CNPq). This support is gratefully acknowledged. The authors would like to thank the anonymous reviewers whose comments helped to improve the final version of this paper.

References

[1] S. Ghannadpour, P. Kiani, J. Reddy, Pseudo spectral method in nonlinear analysis of relatively thick imperfect laminated plates under end-shortening strain, Compos. Struct. 182 (2017) 694–710, https://doi.org/10.1016/J.COMPSTRUCT.2017.08.076.

[2] H. Ersoy, K. Mercan, Ö. Civalek, Frequencies of FGM shells and annular plates by the methods of discrete singular convolution and differential quadrature methods, Compos. Struct. 183 (2018) 7–20, https://doi.org/10.1016/J.COMPSTRUCT.2016.11.051.

[3] K. Mercan, A.K. Baltacıoglu, Ö. Civalek, Free vibration of laminated and FGM/CNT composites annular thick plates with shear deformation by discrete singular convolution method, Compos. Struct. 186 (2018) 139–153, https://doi.org/10.1016/J.COMPSTRUCT.2017.12.008.

[4] A.K. Nor Hafizah, K.K. Viswanathan, Z.A. Aziz, J.H. Lee, Vibration of antisymmetric angle-ply composite annular plates of variable thickness, J. Mech. Sci. Technol. 32 (5) (2018) 2155–2162, https://doi.org/10.1007/s12206-018-0424-1.

[5] K.K. Żur, Free vibration analysis of elastically supported functionally graded annular plates via quasi-Green's function method, Compos. B Eng. 144 (2018) 37–55, https://doi.org/10.1016/J.COMPOSITESB.2018.02.019.

[6] K.K. Żur, Quasi-Green's function approach to free vibration analysis of elastically supported functionally graded circular plates, Compos. Struct. 183 (2018) 600–610, https://doi.org/10.1016/J.COMPSTRUCT.2017.07.012.

[7] S. Brischetto, F. Tornabene, Advanced GDQ models and 3D stress recovery in multilayered plates, spherical and double-curved panels subjected to transverse shear loads, Compos. B Eng. 146 (2018) 244–269, https://doi.org/10.1016/J.COMPOSITESB.2018.04.019.

[8] F. Tornabene, N. Fantuzzi, M. Bacciocchi, Strong and weak formulations based on differential and integral quadrature methods for the free vibration analysis of composite plates and shells: convergence and accuracy, Eng. Anal. Bound. Elem. 92 (2018) 3–37, https://doi.org/10.1016/J.ENGANABOUND.2017.08.020.

[9] F. Tornabene, N. Fantuzzi, M. Bacciocchi, E. Viola, Mechanical behavior of damaged laminated composites plates and shells: higher-order Shear Deformation Theories, Compos. Struct. 189 (2018) 304–329, https://doi.org/10.1016/J.COMPSTRUCT.2018.01.073.

[10] T.J. Hughes, J.A. Cottrell, Y. Bazilevs, Isogeometric analysis: CAD, finite elements, NURBS, exact geometry and mesh refinement, Comput. Methods Appl. Mech. Eng. 194 (39–41) (2005) 4135–4195, https://doi.org/10.1016/j.cma.2004.10.008.

[11] J.A. Cottrell, T.J.R. Hughes, Y. Bazilevs, Isogeometric Analysis: toward Integration of CAD and FEA, John Wiley & Sons Ltd, Chichester, UK, 2009.

[12] D.J. Benson, Y. Bazilevs, M.C. Hsu, T.J.R. Hughes, Isogeometric shell analysis: the Reissner–Mindlin shell, Comput. Methods Appl. Mech. Eng. 199 (5–8) (2010) 276–289 https://doi.org/10.1016/j.cma.2009.05.011.

[13] M.J. Borden, M.A. Scott, J.A. Evans, T.J.R. Hughes, Isogeometric finite element data structures based on Bézier extraction of NURBS, Int. J. Numer. Methods Eng. 87 (1–5) (2011) 15–47, https://doi.org/10.1002/nme.2968.

[14] L. Espath, A. Braun, A. Awruch, S. Maghous, NURBS-based three-dimensional analysis of geometrically nonlinear elastic structures, Eur. J. Mech. A Solid. 47 (2014) 373–390, https://doi.org/10.1016/J.EUROMECHSOL.2014.05.005.

[15] J. Kiendl, F. Auricchio, L. Beirão da Veiga, C. Lovadina, A. Reali, Isogeometric collocation methods for the Reissner–Mindlin plate problem, Comput. Methods Appl. Mech. Eng. 284 (2015) 489–507, https://doi.org/10.1016/J.CMA.2014.09.011.

[16] W. Dornisch, R. Müller, S. Klinkel, An efficient and robust rotational formulation for isogeometric Reissner–Mindlin shell elements, Comput. Methods Appl. Mech. Eng. 303 (2016) 1–34, https://doi.org/10.1016/J.CMA.2016.01.018.

[17] J. Huang, N. Nguyen-Thanh, K. Zhou, Extended isogeometric analysis based on Bézier extraction for the buckling analysis of Mindlin–Reissner plates, Acta Mech. 228 (9) (2017) 3077–3093, https://doi.org/10.1007/s00707-017-1861-0.

[18] J. Kiendl, E. Marino, L. De Lorenzis, Isogeometric collocation for the Reissner–Mindlin shell problem, Comput. Methods Appl. Mech. Eng. 325 (2017) 645–665, https://doi.org/10.1016/J.CMA.2017.07.023.

[19] L.A. Piegl, W. Tiller, The NURBS Book, Springer, 1997.

[20] H. Kapoor, R. Kapania, Geometrically nonlinear NURBS isogeometric finite element analysis of laminated composite plates, Compos. Struct. 94 (12) (2012) 3434–3447, https://doi.org/10.1016/J.COMPSTRUCT.2012.04.028.

[21] T. Le-Manh, J. Lee, Postbuckling of laminated composite plates using NURBS-based isogeometric analysis, Compos. Struct. 109 (2014) 286–293, https://doi.org/10.1016/J.COMPSTRUCT.2013.11.011.

[22] N. Nguyen-Thanh, J. Muthu, X. Zhuang, T. Rabczuk, An adaptive three-dimensional RHT-splines formulation in linear elasto-statics and elasto-dynamics, Comput. Mech. 53 (2) (2014) 369–385, https://doi.org/10.1007/s00466-013-0914-z.

[23] L.V. Tran, J. Lee, H. Nguyen-Van, H. Nguyen-Xuan, M.A. Wahab, Geometrically nonlinear isogeometric analysis of laminated composite plates based on higher-order shear deformation theory, Int. J. Non-Linear Mech. 72 (2015) 42–52, https://doi.org/10.1016/J.IJNONLINMEC.2015.02.007.

[24] T.T. Yu, S. Yin, T.Q. Bui, S. Hirose, A simple FSDT-based isogeometric analysis for geometrically nonlinear analysis of functionally graded plates, Finite Elem. Anal. Des. 96 (2015) 1–10, https://doi.org/10.1016/J.FINEL.2014.11.003.

[25] N. Fantuzzi, F. Tornabene, Strong Formulation Isogeometric Analysis (SFIGA) for laminated composite arbitrarily shaped plates, Compos. B Eng. 96 (2016) 173–203, https://doi.org/10.1016/J.COMPOSITESB.2016.04.034.

[26] F. Tornabene, N. Fantuzzi, M. Bacciocchi, A new doubly-curved shell element for the free vibrations of arbitrarily shaped laminated structures based on Weak Formulation IsoGeometric Analysis, Compos. Struct. 171 (2017) 429–461, https://doi.org/10.1016/J.COMPSTRUCT.2017.03.055.

[27] Q.X. Lieu, S. Lee, J. Kang, J. Lee, Bending and free vibration analyses of in-plane bi-directional functionally graded plates with variable thickness using isogeometric analysis, Compos. Struct. 192 (2018) 434–451, https://doi.org/10.1016/J.COMPSTRUCT.2018.03.021.

[28] P. Tan, N. Nguyen-Thanh, T. Rabczuk, K. Zhou, Static, dynamic and buckling analyses of 3D FGM plates and shells via an isogeometric-meshfree coupling approach, Compos. Struct. 198 (2018) 35–50, https://doi.org/10.1016/J.COMPSTRUCT.2018.05.012.
[29] W. Li, N. Nguyen-Thanh, K. Zhou, Geometrically nonlinear analysis of thin-shell structures based on an isogeometric-meshfree coupling approach, Comput. Methods Appl. Mech. Eng. 336 (2018) 111–134, https://doi.org/10.1016/J.CMA.2018.02.018.
[30] B. Liu, R.T. Haftka, M.A. Akgün, A. Todoroki, Permutation genetic algorithm for stacking sequence design of composite laminates, Comput. Methods Appl. Mech. Eng. 186 (2–4) (2000) 357–372, https://doi.org/10.1016/S0045-7825(99)90391-2.
[31] M.W. Bloomfield, J.E. Herencia, P.M. Weaver, Enhanced two-level optimization of anisotropic laminated composite plates with strength and buckling constraints, Thin-Walled Struct. 47 (11) (2009) 1161–1167, https://doi.org/10.1016/J.TWS.2009.04.008.
[32] I.B.C.M. Rocha, E. Parente Jr., A.M.C. Melo, A hybrid shared/distributed memory parallel genetic algorithm for optimization of laminate composites, Compos. Struct. 107 (2014) 288–297, https://doi.org/10.1016/J.COMPSTRUCT.2013.07.049.
[33] E.S. Barroso, E. Parente Jr., A.M.C. Melo, A hybrid PSO-GA algorithm for optimization of laminated composites, Struct. Multidiscip. Optim. 55 (6) (2017) 2111–2130, https://doi.org/10.1007/s00158-016-1631-y.
[34] R. Echter, M. Bischoff, Numerical efficiency, locking and unlocking of NURBS finite elements, Comput. Methods Appl. Mech. Eng. 199 (5–8) (2010) 374–382, https://doi.org/10.1016/J.CMA.2009.02.035.
[35] T. Belytschko, H. Stolarski, W.K. Liu, N. Carpenter, J.S. Ong, Stress projection for membrane and shear locking in shell finite elements, Comput. Methods Appl. Mech. Eng. 51 (1–3) (1985) 221–258, https://doi.org/10.1016/0045-7825(85)90035-0.
[36] T.J.R. Hughes, A. Reali, G. Sangalli, Efficient quadrature for NURBS-based isogeometric analysis, Comput. Methods Appl. Mech. Eng. 199 (5–8) (2010) 301–313, https://doi.org/10.1016/J.CMA.2008.12.004.
[37] C. Adam, S. Bouabdallah, M. Zarroug, H. Maitournam, Improved numerical integration for locking treatment in isogeometric structural elements. Part II: plates and shells, Comput. Methods Appl. Mech. Eng. 284 (2015) 106–137, https://doi.org/10.1016/J.CMA.2014.07.020.
[38] K. Sze, X. Liu, S. Lo, Popular benchmark problems for geometric nonlinear analysis of shells, Finite Elem. Anal. Des. 40 (11) (2004) 1551–1569, https://doi.org/10.1016/J.FINEL.2003.11.001.
[39] J.N. Reddy, Mechanics of Laminated Composite Plates and Shells : Theory and Analysis, CRC Press, 2004.
[40] M.A. Crisfield, Essentials, vol. 1, John Wiley & Sons Ltd., 1991.
[41] P. Wriggers, W. Wagner, C. Miehe, A quadratically convergent procedure for the calculation of stability points in finite element analysis, Comput. Methods Appl. Mech. Eng. 70 (3) (1988) 329–347, https://doi.org/10.1016/0045-7825(88)90024-2.
[42] P. Wriggers, J.C. Simo, A general procedure for the direct computation of turning and bifurcation points, Int. J. Numer. Methods Eng. 30 (1) (1990) 155–176, https://doi.org/10.1002/nme.1620300110.
[43] E. Parente Jr., A.S. Holanda, S.M.B.A. Silva, Tracing nonlinear equilibrium paths of structures subjected to thermal loading, Comput. Mech. 38 (6) (2006) 505–520, https://doi.org/10.1007/s00466-005-0004-y.
[44] B. Oesterle, E. Ramm, M. Bischoff, A shear deformable, rotation-free isogeometric shell formulation, Comput. Methods Appl. Mech. Eng. 307 (2016) 235–255, https://doi.org/10.1016/J.CMA.2016.04.015.
[45] P. Hu, Q. Hu, Y. Xia, Order reduction method for locking free isogeometric analysis of Timoshenko beams, Comput. Methods Appl. Mech. Eng. 308 (2016) 1–22, https://doi.org/10.1016/J.CMA.2016.05.010.
[46] Efficient isogeometric NURBS-based solid-shell elements: mixed formulation and *B*-method, Comput. Methods Appl. Mech. Eng. 267 (2013) 86–110, https://doi.org/10.1016/J.CMA.2013.08.002.
[47] Simulia, ABAQUS/Standard User's Manual, (2012).
[48] P. Sundaresan, G. Singh, G. Rao, Buckling and post-buckling analysis of moderately thick laminated rectangular plates, Comput. Struct. 61 (1) (1996) 79–86, https://doi.org/10.1016/0045-7949(96)00010-7.
[49] K. Liew, J. Wang, M. Tan, S. Rajendran, Postbuckling analysis of laminated composite plates using the mesh-free kp-Ritz method, Comput. Methods Appl. Mech. Eng. 195 (7–8) (2006) 551–570, https://doi.org/10.1016/J.CMA.2005.02.004.
[50] C.L. Dym, Stability Theory and its Applications to Structural Mechanics, Noordhoff International Publishing Company, 1974 Republished by Dover Publications, 2002).
[51] A. Sabir, A. Lock, The applications of finite elements to large deflection geometrically nonlinear behaviour of cylindrical shells, in: C. Brebbia, H. Tottenham (Eds.), Variational Methods in Engineering, Vol. 2, Southampton Univ. Press, Surrey, England, U.K., 1972, pp. 7/66–67/75.
[52] B.L. Wardle, Solution to the incorrect benchmark shell-buckling problem, AIAA J. 46 (2) (2008) 381–387, https://doi.org/10.2514/1.26698.
[53] Y. Zhou, I. Stanciulescu, T. Eason, M. Spottswood, Nonlinear elastic buckling and postbuckling analysis of cylindrical panels, Finite Elem. Anal. Des. 96 (2015) 41–50, https://doi.org/10.1016/J.FINEL.2014.12.001.